European Journal of Pharmaceutical Sciences 204 (2025) 106944

Contents lists available at ScienceDirect

European Journal of Pharmaceutical Sciences

journal homepage: www.elsevier.com/locate/ejps

Towards a switchable nanoparticle behavior using inverse electron-demand Diels-Alder chemistry and ectoenzyme-based ligand activation

Johannes Lang, Kathrin Schorr, Achim Goepferich *

Department of Pharmaceutical Technology, University of Regensburg, Regensburg, 93053, Germany

ARTICLE INFO

Keywords:
PEG-PLA copolymer nanoparticles
Post-functionalization
Inverse electron-demand Diels-Alder (iEDDA) reaction
Ectoenzyme based ligand activation
Switchable nanoparticle avidity
Angiotensin ll type 1 (AT1) receptor

ABSTRACT

Nanoparticles (NPs) as drug delivery platforms encounter numerous obstacles on their journey from administration to the target site. Often, diametrically opposing particle properties are desirable to overcome biological and physical barriers. Therefore, stimuli-responsive NPs have been developed to allow for specific particle adaptation. In this work, it was demonstrated that NPs can be rendered switchable with respect to their interaction with a receptor through an external chemical stimulus. A combination of the inverse electron-demand Diels-Alder (iEDDA) reaction for subsequent NP functionalization and ectoenzyme-based ligand activation allowed for specific particle tailoring. Building on this, a two-step process for target cell recognition was developed. First, NPs were functionalized with Angiotensin-I (Ang-I) as inactive ligand using iEDDA chemistry. At the target site, the ligand was enzymatically processed to Angiotensin-ll (Ang-II) by cellular ectoenzymes. Ang-ll binds as active ligand to the angiotensin ll type 1 (AT1) receptor on the target cell surface. This enzymatic activation aims to minimize the biological effect of the ligand prior to particle binding, while the NP target cell specificity is increased by a two-step recognition with enzymatic processing and receptor binding.

1. Introduction

NPs have gained considerable attention as drug delivery platforms due to their advantageous properties, including enhanced stability and solubility of encapsulated payloads, as well as reduced systemic toxicity (Mitchell et al., 2021). As a result, research in the field of NP-based drug delivery has seen a steady increase in recent years (Zhao et al., 2019). Typically, NPs retain their size, shape, and surface properties during the journey through the organism. However, this rigid design limits the ability of NPs to adapt to the diverse physical and biological barriers (Li et al., 2022). Following intravenous administration, NPs face several challenges that can impede their delivery, such as blood flow dynamics and clearance by the reticuloendothelial system (RES). Upon reaching target tissues, extravasation and cellular internalization present further barriers, and even after successful uptake, intracellular trafficking may affect the final delivery of the payload (Blanco et al., 2015). Throughout this journey from administration to the target site, NP properties like size, shape, surface charge, and functionalization play pivotal roles (Zhao et al., 2019). However, different stages of this journey often require distinct and sometimes contradictory NP properties (Lu et al., 2023). For instance, NPs require stealth surfaces to evade RES clearance. Yet, these same stealth properties may hinder the effective internalization of NPs once they reach their target cells (Jin et al., 2019).

To address this challenge and tailor NPs to specific situations, stimuli-responsive NPs have been developed (Mura et al., 2013; Crucho, 2015). In cancer therapy, for instance, one can leverage the acidic and

Abbreviations: ^{1}H NMR, proton nuclear magnetic resonance; ACE, angiotensin converting enzyme; Ang-I, angiotensin I; Ang-II, angiotensin II; AT1R, angiotensin II receptor type 1; ATP, adenosine triphosphate; BCA, bicinchoninic acid; $CDCl_3$, deuterated chloroform; DBU, 1,8-diazabicyclo[5.4.0]undec-7-ene; DIPEA, N,N-diisopropylethylamine; DMF, dimethylformamide; DMSO, dimethyl sulfoxide; DPBS, Dulbecco's phosphate buffered saline; EC_{50}, half maximal effective concentration; EDC, 1-ethyl-3-(3-dimethylaminopropyl)carbodiimide; EGTA, ethylene glycol-bis(β-aminoethyl ether)-*N,N,N′,N′*-tetraacetic acid; FBS, fetal bovine serum; HBTU, hexafluorophosphate benzotriazole tetramethyl uranium; IC_{50}, half maximal inhibitory concentration; iEDDA, inverse electron-demand Diels–Alder reaction; MeCN, acetonitrile MWCO, molecular weight cutoff; NHS, N-hydroxysuccinimide; NP, nanoparticle; NTA, nanoparticle tracking analysis; OAT, organic anion transporter; PDI, polydispersity index; PEG, polyethylene glycol; PET, positron emission tomography; PLA, polylactide; PLGA, poly(lactic-co-glycolic acid); RES, reticuloendothelial system; rMCs, rat mesangial cells; ROS, reactive oxygen species; rpm, revolutions per minute; SEC, size-exclusion chromatography; TCO, trans-cyclooctene; Tz, tetrazine.

* Corresponding author.
E-mail address: achim.goepferich@ur.de (A. Goepferich).

https://doi.org/10.1016/j.ejps.2024.106944
Received 16 July 2024; Received in revised form 18 October 2024; Accepted 22 October 2024
Available online 24 October 2024

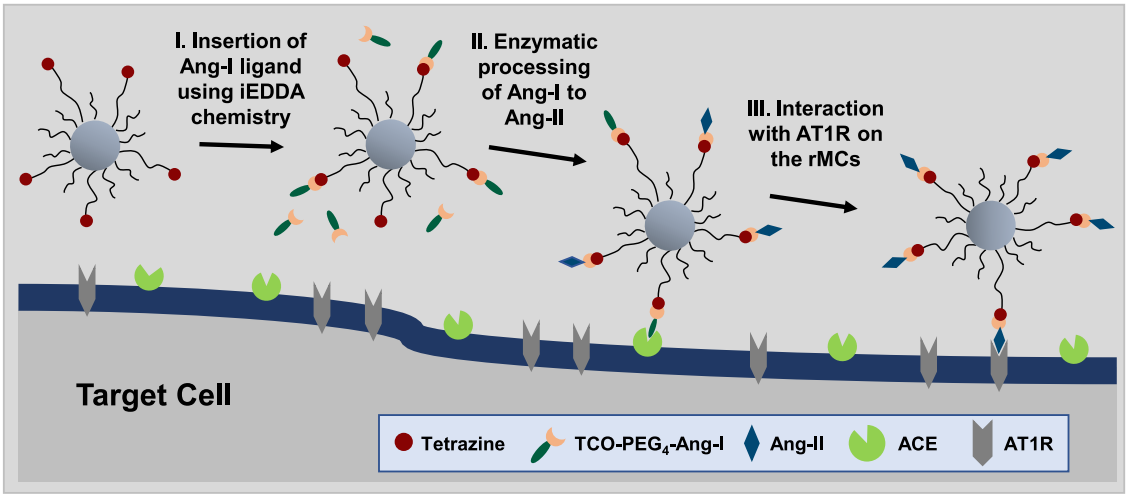

Fig. 1. Schematic representation of the concept to render NPs switchable in their avidity for the AT1 receptor through post-functionalization using the iEDDA reaction and ectoenzyme-based ligand activation.

hypoxic environment of the tumor and design pH- or hypoxia-responsive NPs (Su et al., 2023). Other endogenous triggers include high levels of enzymes (Yao et al., 2018; He et al., 2021), reactive oxygen species (ROS) (Cao et al., 2021; Wang et al., 2019), or adenosine triphosphate (ATP) (Deng and Walther, 2020; Yu et al., 2022). Additionally, exogenous triggers can be used to modify the particles. Essentially, photo- (Tao et al., 2020), thermal- (Sponchioni et al., 2019), and ultrasound-responsive (Tu et al., 2021) NPs are considered in this context. These designs allow for the modification of key NP properties in response to designated stimuli (Lu et al., 2023). Furthermore, cell uptake-promoting ligands can be activated by a stimulus. Several approaches to achieve this controlled ligand activation have been discussed in the literature (Li et al., 2022). Commonly, NPs are fully equipped with all functional components at the time of administration. The ligand for active targeting is often concealed and revealed through the cleavage of a component in response to a specific stimulus (Li et al., 2015; Jin et al., 2013). However, such methods may lack temporal precision, potentially exposing targeting ligands prematurely or before the NP has reached its target site.

In contrast, the present study aims to lay the groundwork for an approach where NPs can be modified in a controlled, constructive manner near the target site. To achieve this, an *in vivo*-compatible bioorthogonal click reaction was assessed to functionalize the NPs. The [4+2] cycloaddition of tetrazine (Tz) and trans-cyclooctene (TCO), known as the inverse electron-demand Diels-Alder (iEDDA) reaction, is particularly suitable for this application due to the extremely fast reaction even at low concentrations and its selectivity in the multitude of functional groups of the organism (Oliveira et al., 2017). While the iEDDA reaction has primarily been employed for *in vivo* particle functionalization in the context of pre-targeted imaging, where radiotracers for positron emission tomography (PET) are attached to NPs post-accumulation in tumors (Idiago-López et al., 2021), its potential for use in stimuli-responsive drug delivery systems has yet to be fully explored. In this study, we sought to demonstrate that the iEDDA reaction can enable the switchable activation of NPs. The delayed addition of a ligand - acting as a chemical stimulus - could serve as a novel mechanism to initiate receptor-mediated target cell recognition. This approach would offer unique control over the timing of ligand activation rendering the NP delivery process in future applications more controllable.

The feasibility of this approach was investigated *in vitro* using angiotensin as an exemplary ligand targeting the angiotensin II type 1 receptor (AT1R) on mesangial cells (Hennig et al., 2015). Angiotensin-I (Ang-I), modified with TCO for the iEDDA reaction, was designed to react with Tz-functionalized NPs. Once bound to the NP surface, Ang-I required further activation by the membrane-bound ectoenzyme angiotensin-converting enzyme (ACE) to convert into the active form, Angiotensin-II (Ang-II) (Maslanka Figueroa et al., 2019). This additional activation step was included to minimize the biological activity of the ligand prior to processing. Moreover, the dual requirement of ACE and the AT1 receptor on target cells may further increase the specificity of NP targeting. The combination of the iEDDA reaction and ectoenzyme-mediated ligand activation provided a new strategy for creating NPs with switchable targeting properties (see Fig. 1). This stimuli-responsive design holds promise for future *in vivo* applications, where non-functionalized NPs could initially exploit their stealth properties to evade immune recognition, followed by temporally controlled ligand activation to promote specific cellular uptake. The presented concept, utilizing a two-step activation process, could potentially open new avenues for enhancing target specificity and thus therapeutic efficacy in NP-based drug delivery.

2. Materials and methods

2.1. Materials

PEG derivatives (COOH-PEG2k-OH, mPEG2k-OH, COOH-PEG5k-OH and tBoc-NH-PEG5k-OH) were obtained from JenKem Technology USA Inc (Allen, TX, USA). Lysine N-modified Ang-I and Ang-II (Lys-Ang-I Sequence KDRVYIHPFHL and Lys-Ang-II Sequence KDRVYIHPF) were synthesized according to order from Genscript (Piscataway, NJ, USA). The nitrile 3-(4-cyanophenyl)-propionic acid as starting compound for the synthesis of tetrazine was purchased from abcr GmbH (Karlsruhe, Germany). TCO-PEG_4-NHS ester (axial isomer) was obtained from Lumiprobe (Hannover, Germany). The cellulose dialysis membranes, which were used to purify the polymers after ligand coupling, were purchased from Spectrum Laboratories Inc (Rancho Dominguez, CA, USA). NP solutions were concentrated with centrifugal devices (30 or 100 kDa molecular weight cutoff) which were purchased from Pall Life Sciences (Portsmouth, UK). QuantiPro™ BCA assay kit for angiotensin

quantification, angiotensin-converting enzyme from rabbit lung (≥2.0 units/mg protein (modified Warburg-Christian)) for enzymatic activation and RPMI-1640 medium and hydrocortisone for cell culture were obtained from Sigma Aldrich (Taufkirchen, Germany). Fetal bovine serum (FBS, South America origin, 0.2 μm sterile filtered, Lot No.: P201004) was sourced from PAN Biotech GmbH (Aidenbach, Germany) and insulin-transferrin-selenium was purchased from Life Technologies Corporation (Grand Island, NY, USA). Fura-2 AM as ratiometric Ca^{2+} indicator was ordered from Thermo Fisher Scientific (Waltham, MA, USA). All other materials were reagent grade and obtained from Merck KGaA (Darmstadt, Germany). Millipore water was generated using a Milli-Q water purification system (Millipore, Schwalbach, Germany).

2.2. Polymer synthesis and ligand coupling

The PLA-PEG block copolymers with diverse functional groups were synthesized using the respective carboxylic acid-, amine-, or methoxy-terminated PEG derivatives as macroinitiators, as previously reported by our group (Abstiens et al., 2019). The ring-opening polymerization of cyclic lactide, using 1,8-diazabicyclo[5.4.0]undec-7-ene (DBU) as a catalyst, yielded copolymers with approximately 10 kDa PLA and 2 kDa or 5 kDa PEG chains with the corresponding functional group on the PEG depending on the chosen starting material. More detailed information regarding the synthesis of the copolymers and ^{1}H NMR spectra for characterization can be found in the SI section I. The ligand coupling was performed using peptide chemistry with either hexafluorophosphate benzotriazole tetramethyl uronium (HBTU) or 1-ethyl-3-(3-dimethylaminopropyl)carbodiimide (EDC)/ N-hydroxysuccinimide (NHS) as coupling reagents and N,N-diisopropylethylamine (DIPEA) as base in dimethylformamide (DMF). Tetrazine with carboxy functionality was coupled to the PLA10k-PEG5k-NH_2 block copolymer using HBTU. For the coupling of the Angiotensin ligands Ang-I and Ang-II, PLA10k-PEG5k--COOH was activated with EDC/NHS, excess EDC was quenched with 2-mercapthoethanol, and the Angiotensin ligands were subsequently added. Reaction times were sufficiently long to allow for complete coupling. The reaction mixtures were then precipitated in a 10-fold volume of ice-cold diethyl ether and centrifuged at 4 °C. The supernatant was discarded, and the pellet was dried before being dissolved in acetonitrile. This precipitation-centrifugation-dissolution cycle was repeated once more. The pellets were dissolved in MeCN, the polymer solutions were dropwise added into vigorously stirring Millipore water, and the polymer micelles were stirred for approximately 2 hours. Further purification was achieved through dialysis (RC, 6–8 kDa MWCO) against 4 L Millipore water. Finally, the ligand-functionalized block copolymers were lyophilized for 3 days. For product characterization, a ^{1}H NMR in $CDCl_3$ or DMSO-d6 was recorded on a Bruker Avance III HD 400 (Bruker BioSpin GmbH, Rheinstetten, Germany). Details regarding ligand coupling, ^{1}H NMR for characterization, and determination of coupling efficiency can be found in the SI Section III.

2.3. NP preparation and characterization

A 10 mg/mL solution with a PEG-PLA block copolymer to particle-core-forming poly(lactic-co-glycolic acid) (PLGA) mass ratio of 70:30 in acetonitrile was prepared. The copolymer fraction was adjusted to ensure that 20 % of the PEG-PLA copolymers carried the ligand (PLA10k-PEG5k-Tz, -Ang-I, or -Ang-II), with PLA10k-PEG2k-COOH serving as the filler polymer. NPs were prepared via bulk nanoprecipitation, wherein the polymer solution in acetonitrile (10 mg/mL) was added dropwise to vigorously stirred (800 rpm) Millipore water (Abstiens and Goepferich, 2019). The NPs were left stirring for 3 h until the organic solvent (MeCN) was completely evaporated. The resulting 1 mg/mL NP solution was concentrated through centrifugation using a 100-kDa molecular weight cutoff Microsep advance centrifugal device (Pall Life Sciences) for 30 minutes at 3000 g. Subsequently, NP size and concentration were determined in Millipore water using nanoparticle tracking analysis (NTA) on a NanoSight NS300 (Malvern Panalytical GmbH, Kassel, Germany) (Filipe et al., 2010). The dilution was adjusted so that between 10 and 50 particles per frame could be measured and the detection threshold in the evaluation was set to 3. Unless otherwise stated, the mode value given by NanoSight NS300 is reported as the hydrodynamic diameter of the particles. The polydispersity index (PDI) was calculated from the NTA data according to Clayton et al. (2016) using the following formula (Eq. (1)).

$$PDI = \left(\frac{\sigma}{d}\right)^2 \quad (1)$$

The PDI results from the standard deviation σ of the particle diameter distribution divided by the mean particle diameter d. The molar NP concentration was determined based on the particle concentration (particles/mL) output by the instrument using Avogadro's number. The zeta potential of 1 nM NPs was measured in 10 % PBS at 25 °C on a Malvern ZetaSizer Nano ZS (Malvern Instruments GmbH, Kassel, Germany).

2.4. Quantification of ligands per NP

For the quantification of tetrazine ligands per NP, 50 μL of the concentrated NP sample was dispensed into a transparent 384-well plate (Corning, Corning, NY, USA) and diluted with 50 μL dimethyl sulfoxide (DMSO) to initiate NP dissolution. For the calibration curve, 50 μL of free tetrazine diluted to different concentrations in DMSO was added to 50 μL of Millipore water (tetrazine total concentration in the well 100–500 μM). The absorbance at the absorption maximum of tetrazine at λ 532 nm was measured on a FLUOstar Omega microplate reader (BMG Labtech, Ortenberg, Germany). The tetrazine concentration in the NP sample, determined using the calibration curve, was referenced to the NP concentration determined through nanoparticle tracking analysis, thus quantifying the number of tetrazine ligands per particle.

Ang-I or -II ligands per NP were quantified using a BCA assay following the manufacturer's protocol for the QuantiPro™ BCA Assay Kit. For calibration, free Lys-Ang-I or -II was diluted from a 10 mM solution in DMSO to suitable concentrations in Millipore water (15–75 μM Angiotensin). 40 μL of the calibration solution or the sample with a 10 nM NP solution was dispensed into a transparent 384-well plate. Subsequently, 40 μL of QuantiPro working reagent per well were added, and the solution was mixed by pipetting up and down. The plate was sealed with a plate sealer and incubated at 60 °C for 1 h. The absorption at λ 562 nm was immediately determined using a FLUOstar Omega microplate reader. Similar to the tetrazine ligands, the angiotensin concentration calculated via the calibration curve was referenced to the NP concentration.

In both cases, the surface area of the particles was additionally calculated from the hydrodynamic diameter of the NPs, assuming a spherical shape. This, along with the number of ligands per NP, was used to determine the ligand density.

2.5. Investigation of iEDDA reaction kinetics

TCO-PEG_4-COOH was diluted from a stock solution in DMSO into the wells of a 96-well quartz plate (Hellma GmbH, Müllheim, Germany) with water, resulting in 2, 4, 8, 16, and 32-fold excess relative to tetrazine. The DMSO content in all wells was adjusted to 4 % (v/v). Tetrazine (either free in solution, on polymer micelles, or on NPs) was added via the plate reader's pump system to achieve a final tetrazine concentration of 10 μM per well. The micelles, like the NPs, were functionalized with 20 % tetrazine but did not contain core-forming PLGA. Immediately after automated addition, the decrease in tetrazine absorbance at λ 276 nm was monitored (0.3 s kinetic interval time; 25 °C). Data were fitted with an exponential decay, yielding pseudo-first-order rate constants (k_{obs}). The k_{obs} values were plotted against the TCO concentration, and a linear fit was performed. The slope of the line

yields the second-order rate constant.

2.6. Cell culture

Rat mesangial cells (rMCs) were generously provided by Professor Dr. Armin Kurtz (Institute of Physiology at the University of Regensburg, Regensburg, Germany). The cell line was selected as the target cells due to their stable AT1R expression, as previously demonstrated in studies conducted by our research group (Hennig et al., 2015; Maslanka Figueroa et al., 2019; Zimmer and Goepferich, 2023). The cells were cultured in RPMI 1640 medium supplemented with 10 % fetal bovine serum, insulin-transferrin-selenium, and 100 nM hydrocortisone and in T-75 cell culture flasks (Corning, Corning, NY, USA) at 37 °C with a 5 % CO_2 atmosphere.

2.7. Fura-2 AM-based Ca^{2+} mobilization assay

To investigate the affinity of the ligands, both in their free form and NP-bound, towards the AT1R, a ratiometric Fura-2 AM Ca^{2+} assay as previously reported by our group was used (Zimmer and Goepferich, 2023). 50 µg of Fura-2 AM were dissolved in 50 µL of DMSO. From this stock solution, the Fura-2 AM loading medium was prepared by combining the 50 µL stock solution with 20 µL of a 20 % Pluronic F127 solution and diluting it to a final volume of 6 mL in Leibovitz's medium containing 2.5 mM Probenecid. The rMCs at passages 78 or 79 were allowed to grow in a T75 cell culture flask at 37 °C in the CO_2 incubator until they reached at least 90 % confluence. On the day of the experiment, the cells were washed with 10 mL of DPBS and harvested by incubation with 0.25 % trypsin. Subsequently, 9 mL of serum-containing medium was added, and the cells were centrifuged at 200 rcf for 5 minutes using a 5702 R centrifuge (Eppendorf, Germany). The supernatant was discarded, and the cell pellet was gently resuspended in the Fura-2 AM loading medium. The rMCs were incubated for 1 h at room temperature on a laboratory shaker at 50 rpm, protected from light. The Fura-2 AM-loaded cells were centrifuged using the settings mentioned earlier, and the loading medium was removed. The cells were carefully (so as not to expose the cells to shear stress) resuspended in a measurement buffer based on Leibovitz's medium containing 2.5 mM OAT inhibitor Probenecid. The cell number was determined using a Neubauer-improved counting chamber (Marienfeld, Germany) and adjusted to 1 million rMCs per mL.

In the direct procedure to determine EC_{50} values, the cell suspension was immediately used for measurements on the FLUOstar Omega plate reader. 90 µL of Fura-2 AM-loaded cells were added to 10 µL of the sample (in 10 % PBS) via the plate reader's pump system with a low pump speed of 100 µL/s to minimize mechanical impact/shearing. In the approach described in this paper as the inverse procedure, the ligand for the AT1 receptor was first incubated with the Fura-2 AM-loaded cells. After a specified time interval, free Lys-Ang-II was added through the plate reader's pump system to stimulate the cells. In this case, the focus is not on examining the calcium influx caused by the binding of the ligand to the AT1R but, conversely, assessing the extent to which the Lys-Ang-II signal could be reduced. This serves as a measure of AT1R binding by the previously added ligand. In the inverse procedure applied to determine IC_{50} values, 90 µL of the cell suspension were incubated for 1 h with 10 µL of the ligands in 10 % PBS, either in their free or NP-bound form. Cell stimulation was then carried out using 100 µL of a 300 nM Lys-Ang-II solution in 10 % PBS. The inverse procedure was also used to examine the kinetics of the enzymatic processing and subsequent AT1R interaction of the angiotensin ligands on the rMCs. For this purpose, 90 µL of Fura-2-loaded rMCs in suspension were incubated with 50 µL of the free ligand TCO-PEG_4-Ang-I (10 µM total concentration of free ligand) or 60 µL of the respective NPs in 10 % PBS (2 nM total concentration of NPs) for varying durations at 37 °C under gentle agitation. For measurements, cells were stimulated in this case with 50 µL of the free agonist Lys-Ang-II (1 µM solution in 10 % PBS). A compilation illustrating the experimental procedure for the direct and inverse approach can be found in **SI Table 1**.

Both in the direct and in the inverse procedure the fluorescence intensity was measured for 30 seconds whereby the sample was alternately excited at λ 340 and λ 380 nm, and emission at λ 510 nm was detected. The highest measured ratio R between the resulting fluorescence under excitation at λ 340 and λ 380 nm was utilized to calculate the intracellular calcium concentration [Ca^{2+}] applying the Grynkiewicz equation (Eq. (2)) (Grynkiewicz et al., 1985).

$$\left[Ca^{2+}\right] = K_d \left(\frac{R - R_{min}}{R_{max} - R}\right)\left(\frac{S_{f2}}{S_{b2}}\right) \tag{2}$$

To determine the maximum ratio R_{max}, 90 µL of Fura-2 AM-loaded cells introduced via the pump system were lysed with 10 µL of 1 % Triton X-100 in PBS. The minimum ratio R_{min} was determined using 10 µL of 1 % Triton X-100 in PBS supplemented with 45 mM EGTA in 0.5 M NaOH to chelate the total Ca^{2+} with EGTA as the chelating agent. S_{f2} represents the maximum emission of free Fura-2 AM (determined after cell lysis and Ca^{2+} chelation with EGTA) and S_{b2} stands for the maximum emission of Fura-2 AM with bound Ca^{2+} (determined after cell lysis, but without chelation of Ca^{2+}), in each case at an exication wavelength of λ 380 nm. The value for 10 % PBS as blank was subtracted from all intracellular calcium concentrations calculated via the Grynkiewicz equation (Eq. (2)) and the values were normalized against the highest concentration. Experimental data were fitted using a four-parameter nonlinear regression model (Eq. (3)) to obtain binding curves and EC_{50} or IC_{50} values. For the fit of binding curves where the corresponding plateau could not be reached, the bottom asymptote A1 was set to 0 (Fig. 6 A curve for NP-Ang-I and NP-Tz-TCO-Ang-I) or the top asymptote $A2$ to 100 (Fig. 4 C curve for NP-Tz-TCO-Ang-I and NP-Tz-TCO-Ang-I + ACE). Further, x0 stands for the EC_{50} or IC_{50} value and p represents the hill slope describing the steepness of the curves.

$$y = A1 + \frac{A2 - A1}{1 + 10^{(LOGx0 - x)\ p}} \tag{3}$$

In the kinetics experiments, the extent to which the Lys-Ang-II signal could be reduced provides insights into the degree of AT1R saturation by the free ligand or NPs, thus allowing assessments of ligand/NP-cell interactions. The kinetics of AT1R saturation were fitted with Eq. 4 for an exponential plateau, where y_0 stands for the initial value and yS for the saturation value and k is a rate constant.

$$y = y_S - \left(y_S - y_0\right) \cdot e^{-kx} \tag{4}$$

2.8. Post-Functionalization, enzymatic activation and NP avidity for the AT1R

To functionalize NP-Tz with Ang-l trough iEDDA reaction, a 20 nM NP-Tz solution was incubated with 400 µM TCO-PEG_4-Ang-I for 1 h at 37 °C, followed by the removal of free TCO-modified Ang-I through size-exclusion chromatography (SEC). The SEC was carried out with 4 % Agarose Beads (Agarose Beads Technologies, Madrid, Spain) using a gravity protocol. NP fraction was detected on the Zetasizer (Malvern Panalytical GmbH, Kassel, Germany) and collected accordingly. The NPs were concentrated using a 30-kDa molecular weight cutoff Microsep advance centrifugal device for 30 minutes at 3000 g. To assess the extent of Ang-I removal, a control experiment was conducted using 20 nM NP-COOH incubated with 400 µM TCO-PEG_4-Ang-I, where the absence of tetrazine on the NP prevents covalent binding. Free TCO-modified Ang-I was similarly separated via SEC, and the NPs were concentrated by centrifugation. The concentrated NPs were measured on the Nanosight NS300 in both cases to determine size and NP concentration. The BCA assay for quantifying the Ang-I ligands on the NP was performed as described above, using free Lys-Ang-I as a standard for calibration. The value for the non-functionalized NPs was subtracted from the functionalized NPs as a blank value.

The particles functionalized via iEDDA reaction with Ang-I were tested either directly in a Fura-2 AM Ca^{2+} assay or additionally activated with soluble ACE. A 1 nM NP solution was incubated for 4 hours at 37 °C in DPBS (pH 7.4) with 100 nM soluble ACE. The NPs were concentrated by centrifugation using a 30-kDa molecular weight cutoff centrifugal filter. Subsequently, NP size and concentration were determined using NTA. For the Fura-2 AM Ca^{2+} mobilization assay, the concentrated NP sample was diluted 1:3 and 1:10. These two solutions were further diluted 1:10 and the corresponding dilution series were prepared. 10 µL of the sample were added in triplicate to a white 96-well plate, and the Fura-2 AM Ca^{2+} assay was performed according to the direct procedure as previously described.

To investigate the NP avidity for the AT1R after enzymatic activation not by soluble ACE but by cell membrane-bound enzyme, the Fura-2 AM Ca^{2+} assay was conducted using the inverse procedure. Dilution series were prepared again from the tetrazine-functionalized NPs, the post-functionalized NPs, as well as from directly Ang-I and Ang-II functionalized NPs for comparison. 10 µL of the sample was added in triplicate to a white 96-well plate. The NP solutions were incubated with 90 µL of cell suspension for 1 h at 37 °C, followed by the addition of 100 µL of 300 nM Ang-II solution for stimulation, as described in Section 2.7.

2.9. Data analysis

Fit of experimental data and statistical analysis was performed using Origin software (Version 2020, OriginLab Corporation, Northampton, MA, USA). One-way ANOVA with a Tukey's multiple comparison test was used for statistical evaluation of significance. The number of performed experiments is stated in the figure caption and levels of statistical significance are indicated as *p ≤ 0.05, **p ≤ 0.01, ***p ≤ 0.001, and ****p ≤ 0.0001 in the respective figures.

3. Results and discussion

3.1. Preparation and characterization of PEG-PLA copolymer NPs

Tetrazine-functionalized NPs were synthesized, capable of undergoing an iEDDA reaction with TCO-modified Ang-I. Additionally, blank NP-COOH and directly Ang-I as well as Ang-II functionalized NPs were prepared for comparison. PEG-PLA copolymer particles, well established in our research group, with a PLGA-stabilized core served as excellent model for this study. Pre-functionalization of the polymer with the desired ligand prior to NP formation allows tailoring of NP properties such as size, zeta potential, and particularly ligand density per NP (Maslanka Figueroa et al., 2020). Functionalization was consistently chosen so that 20 % of the PEG-PLA copolymers carry the ligand (tetrazine, Ang-I, or Ang-II). To enhance flexibility and accessibility of the ligands, they were attached to longer PEG5k chains, whereas the spacer chains were designed with PEG2k polymer (see Fig. 2 A). The use of COOH-terminated spacer chains resulted in a negative zeta potential due to the deprotonation of the acid in aqueous solution. The carboxy blank particles exhibited a strongly negative zeta potential of -28 ± 3 mV, whereas tetrazine-functionalized NPs showed a less negative zeta potential of -14.5 ± 0.4 mV due to tetrazine's neutral charge contribution (see Fig. 2 B and **SI Figure 7** A). Particles prepared by nanoprecipitation showed a size in the range of about 60 to 80 nm (see Fig. 2 C, for the size

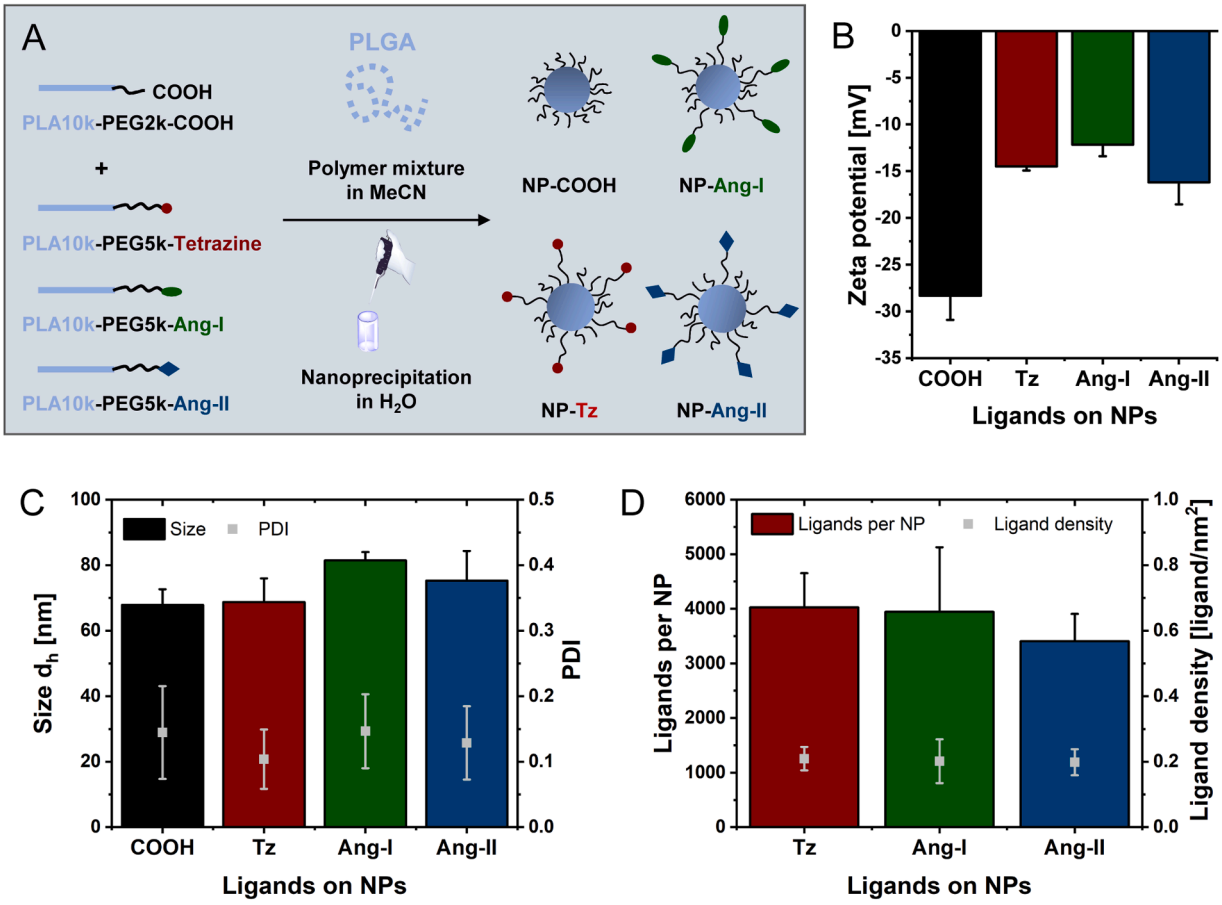

Fig. 2. NP preparation and characterization. (A) Scheme for the preparation of the different NPs. (B) Zeta potential of the NPs in 10 % PBS. Results are presented as mean ± SD of n = 3 measurements. (C) Size and PDI of the NPs measured by NTA. (D) Quantification of ligands per NP and calculated ligand density on the NP. Results in C and D are presented as mean ± SD of at least N = 3 experiments.

distribution of the NPs see also **SI Figure 7** B). The NPs functionalized with Angiotensin were slightly larger than the tetrazine-functionalized or the carboxy blank particles. The PDI was between 0.1 and 0.2 for all NP types, indicating a narrow size distribution. Both the tetrazine-functionalized and angiotensin-functionalized NPs showed around 4000 ligands per particle, corresponding to a ligand density of approximately 0.2 ligands per nm^2 (see Fig. 2 D and **SI Figure 8** for details on the quantification of ligands per NP). Since the PEG density on the NP is very high and the PEG conformation can be assigned to the "dense brush" regime, a backfolding of the long ligand-bearing PEG5k chains towards the particle core is rather unlikely. There should be no room for a loop of the PEG chains, so that ligands could hide in the PEG brush of the particle. Thus, virtually all ligands should be available for interaction with the target cell (see **SI Figure 9** for calculations to estimate the PEG conformation on the particle). In addition, thinking towards the *in vivo* application envisaged in the future, the PEG conformation, being distinctly in the dense brush regime, should be ideally suited to avoid uptake by immune cells and prevent clearance of the NPs (Yang et al., 2014). To summarize, it can be stated that similar zeta potentials, sizes, and ligand densities of the NPs allowed for good comparability among the particles and enabled the observation of effects induced solely by the different ligands.

3.2. iEDDA reaction kinetics on the NP

While numerous studies in the literature confirm the fast kinetics for iEDDA reaction in solution (Darko et al., 2014), this study investigated whether the reaction also proceeds robustly on the copolymer NPs (see Fig. 3 A). To follow the reaction kinetics, the decrease in tetrazine absorbance in the UV range was examined (considerations regarding this can be found in **SI Figure 10**). The change in absorbance with increasing reaction time was fitted with an exponential decay, obtaining pseudo first-order rate constants k_{obs}. These k_{obs} values were plotted against the TCO concentration, with the second-order rate constant derived from the slope of the linear fit. After initially investigating the reaction between free tetrazine in solution and different TCO excesses, micelles and NPs were prepared with 20 % tetrazine functionalization. The micelles did not contain core-forming PLGA and were approximately half the size of the NP-Tz (see Fig. 3 B). The iEDDA reaction was also followed with different TCO excesses. Interestingly, the iEDDA reaction proceeded at an accelerated rate on the NP compared to the reaction in solution although anchoring the tetrazine on the NP or micelle might typically suggest a reduced collision density between tetrazine and TCO (see Fig. 3 C). A possible explanation for the faster reaction on the NP could lie in the hydrophobic nature of the TCO. It is well known that under aqueous conditions, iEDDA reactions are significantly accelerated due to the hydrophobic effect (Darko et al., 2014). On the NP, this effect could be amplified, as the hydrophobic TCO may preferentially accumulate within the PEG brush of the NP to avoid interaction with water. This would result in a locally higher concentration, which could have contributed to the observed faster reaction on the NP. In solution, a second-order rate constant of 492 ± 31 M^{-1} s^{-1} at 25 °C was determined. This value aligns well with rate constants reported in the literature for comparable TCO/tetrazine pairs (Karver et al., 2011). For example, Karver et al. found a second-order rate constant of 820 ± 70 M^{-1} s^{-1} for the reaction of a methyl-substituted tetrazine, which should be comparable to the one used in this study, with TCO at 37 °C. Given the fact that reaction rates can be assumed to double every 10 °C (Leenson, 1999), this would result in a constant of approximately 400 M^{-1} s^{-1} at 25 °C. A second order rate constant of 550 ± 83 M^{-1} s^{-1} was found for the tetrazine on the polymer micelles. This in turn also matches well with the rate constant k_2 of around 600 M^{-1} s^{-1} reported by Kramer et al. for endgroup tetrazine-functionalized polymer micelles at 25 °C (Kramer et al., 2019). On the NP surface, a second-order rate

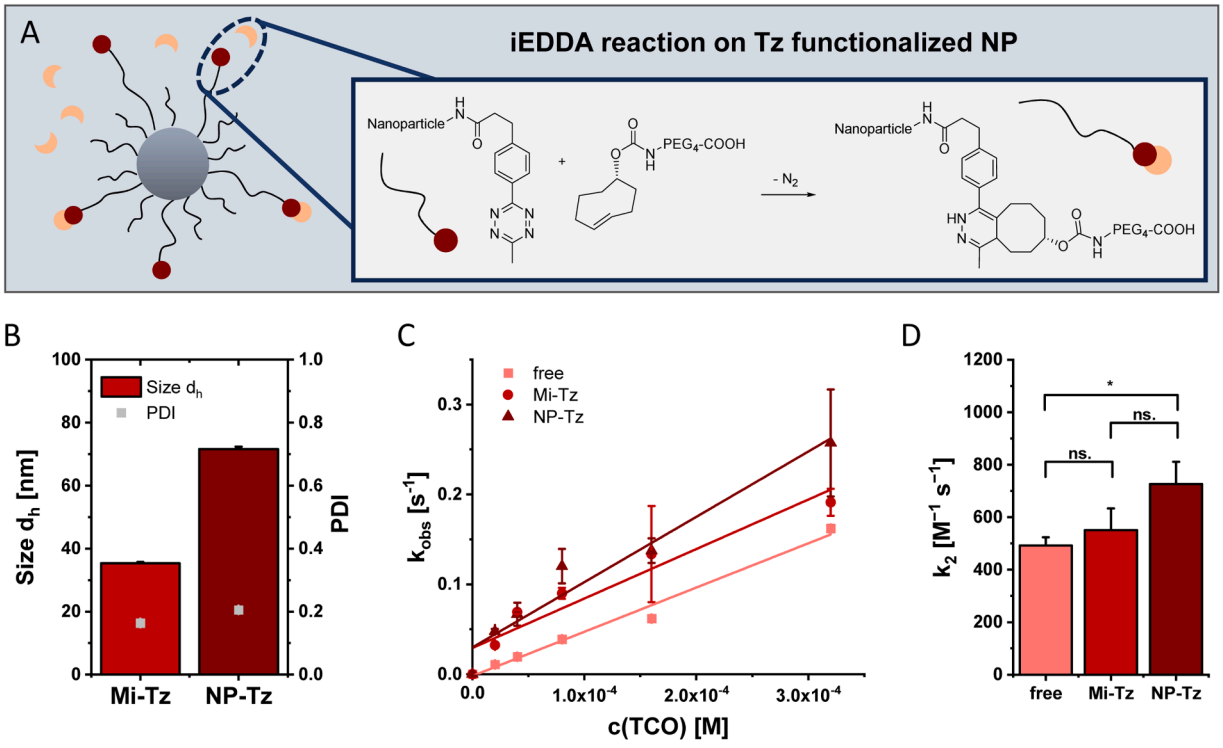

Fig. 3. Investigation of the iEDDA reaction kinetics on the NP. (A) Scheme of the iEDDA reaction between tetrazine functionalized NPs and TCO-PEG_4-COOH. (B) Hydrodynamic diameter and PDI of the tetrazine functionalized micelles (Mi-Tz) and tetrazine functionalized NPs (NP-Tz) determined at the Zetasizer. (C) Plot of the pseudo first-order rate constant (k_{obs}) *vs.* TCO concentration to determine the second-order rate constants. (D) Second-order rate constants for the iEDDA reaction between free tetrazine (free), tetrazine on polymer micelles (Mi-Tz) and tetrazine on NP (NP-Tz), each with TCO-PEG_4-COOH at 25 °C. Results are presented as mean ± SD of $n = 3$ measurements.

constant of 726 ± 85 M^{-1} s^{-1} was determined (see Fig. 3 D). For instance, for 10 μM tetrazine coupled to the NP surface (corresponding to a NP concentration of approximately 2.5 nM) and an 8-fold TCO excess, the reaction was almost completed in less than 30 s. In summary, although the trade-off between reactivity and stability for the methyl-substituted tetrazine used in this study was more on the side of stability, the iEDDA reaction on the NP surface still proceeded rapidly.

3.3. Affinity of free angiotensin ligands for the AT1R

After confirming a rapid iEDDA reaction for subsequent NP functionalization, the interaction of free TCO-PEG_4-Ang-I ligand with the target cell was investigated. TCO-PEG_4-Ang-I was incubated with rMC cell suspension for varying durations, leading to enzymatic processing of Ang-I to Ang-II by cell membrane-bound ACE. The extent of binding to the AT1 receptor following enzymatic activation was determined using an inverse Fura-2 AM Ca^{2+} mobilization assay (Maslanka Figueroa et al., 2020). Cells were stimulated with additional free Ang-II, and the degree to which calcium influx could be suppressed by receptor saturation was measured (for further explanation see **SI Figure 11**). Initially, as expected, no AT1R binding was observed. However, over time, enzymatic processing gradually led to receptor saturation, with a plateau reached after approximately 90 minutes (see Fig. 4 A). In contrast, the iEDDA reaction of an equivalent amount of TCO with tetrazine-functionalized NPs was completed within approximately 5 minutes. Consequently, it was conceivable that the ligand undergoes the iEDDA reaction with tetrazine on the NP prior to experiencing enzymatic activation of Ang-I to Ang-II and subsequent interaction with the AT1R. The rapid kinetics of the iEDDA reaction, in conjunction with the slower enzymatic processing, could facilitate initial particle functionalization *in vitro*. Furthermore, the affinity of free angiotensin ligands for the AT1 receptor was examined. Various dilutions of ligands were incubated with Fura-2 AM loaded cell suspension for 1 h. With Lys-Ang-II, the expected binding curve was observed, yielding an IC_{50} value of 3.5 ± 0.3 nM, consistent with the value reported by Maslanka Figueroa et al. (2020). The binding curves of Lys-Ang-I and TCO-PEG_4-Ang-I were nearly identical (see Fig. 4 B). IC_{50} values of 0.33 ± 0.06 μM for Lys-Ang-I and 0.22 ± 0.06 μM for TCO-PEG_4-Ang-I were determined. The affinity for the AT1R was lower than that for Lys-Ang-II (compare Fig. 4 C), as the ligands first had to be activated by cell membrane-bound ACE (see Fig. 4 D). Comparable IC_{50} values for Lys-Ang-I and TCO-PEG_4-Ang-I suggested that modification of Lys-Ang-I with TCO as a partner of the iEDDA reaction did not interfere with enzymatic processing or receptor binding. **SI Figure 12** additionally provides a comparison with N-terminal acetylated angiotensin. In summary, due to the rapid iEDDA reaction and slower enzymatic processing, it is probable that *in vitro* NP functionalization occurs

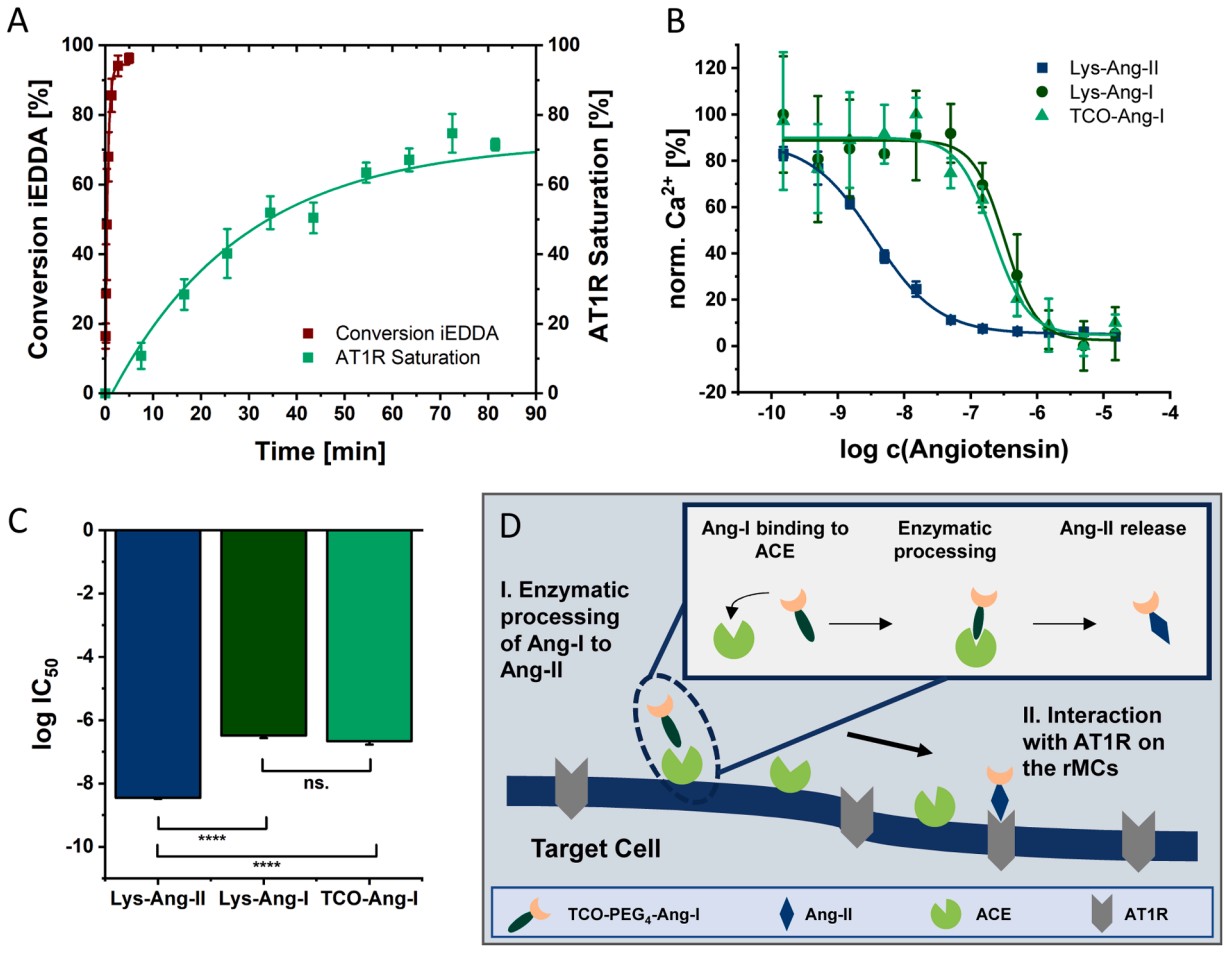

Fig. 4. Interaction of free angiotensin ligands with the AT1 receptor. (A) Comparison of the conversion of the iEDDA reaction with AT1R inhibition. The kinetics of the iEDDA reaction of 10 μM TCO-PEG_4-COOH with an equimolar amount of tetrazine on the NP was investigated by monitoring the decrease in tetrazine absorbance in the UV range (data presented as mean ± SD n=2); AT1R saturation of 10 μM TCO-PEG_4-Ang-I by enzymatic processing of Ang-I to -II and subsequent binding to the receptor was examined by inverse Fura-2 AM Ca^{2+} mobilization assay (data presented as mean ± SD n=3). (B) Affinity of free angiotensin ligands for the AT1R after 1 h incubation with the cells. Binding curves determined via Fura-2 AM Ca^{2+} mobilization assay by inverse stimulation with free Ang-II. Results are presented as mean ± SD of at least n = 3 measurements. (C) logIC_{50} values for the free ligands obtained from the fit of the Fura-2 AM Ca^{2+} assay data. (D) Schematic of the enzymatic activation of TCO-PEG_4-Ang-I and subsequent binding to the AT1R.

initially before free ligand activation. Further, it was demonstrated that TCO modification does not adversely affect affinity, with similar affinities found for Lys-Ang-I and TCO-PEG$_4$-Ang-I for AT1R.

3.4. Post-functionalization of NP-Tz with Angiotensin-I via iEDDA reaction and avidity for the AT1R after Enzymatic activation

To render the NPs switchable concerning their interaction with the AT1R, two fundamental steps had to be implemented. First, the particle had to undergo post-functionalization through the iEDDA reaction. Subsequently, the Ang-I-functionalized NPs had to be enzymatically processed to Ang-II by ACE. The NPs functionalized only with tetrazine were incubated with TCO-PEG$_4$-Ang-I for 1 h to allow sufficient time for the iEDDA reaction on the particle. Excess TCO-PEG$_4$-Ang-I was separated by SEC, and the Ang-I was then quantified using a BCA assay. Based on the NP concentration, the number of Ang-I ligands per NP was determined (see Fig. 5 A). With 3442 ± 303 Ang-I ligands per NP, slightly fewer than tetrazine ligands before functionalization were present, indicating efficient iEDDA reaction on the NP (approx. 86 %). Functionalization with Ang-I resulted in minimal size increase of the NPs from 60 ± 4 nm for NP-Tz to 67 ± 4 nm for NP-Tz-TCO-Ang-I. Subsequently, the post-functionalized NPs were incubated with soluble ACE for 4 hours at 37 °C. The particles were then expected to be fully activated to Ang-II (Maslanka Figueroa et al., 2019). Incubation with soluble ACE resulted in further size increase to 84 ± 6 nm, with the size distribution also becoming significantly broader (compare Fig. 5 B). The NPs were examined for their avidity to the AT1R using a Fura-2 AM Ca^{2+} mobilization assay. The NPs only functionalized with tetrazine showed no Ca^{2+} influx, thus indicating no interaction with the AT1R. In contrast, the post-functionalized and subsequently enzymatically activated particles interact with the receptor (see Fig. 5 C). An EC_{50} value of 2.0 ± 0.5 nM was determined, illustrating sufficient avidity of the NPs (see Fig. 5 D). Surprisingly, the post-functionalized NPs without enzymatic activation showed Ca^{2+} influx at the highest concentrations. This indicates that Ang-I may be converted to Ang-II by membrane-bound ACE within the short measurement period, suggesting that ACE on the cell membrane alone might be sufficient to activate the particles.

3.5. Activation of NPs by cell membrane-bound ACE and kinetics of particle-AT1R interaction

Next, it was investigated whether the particles post-functionalized

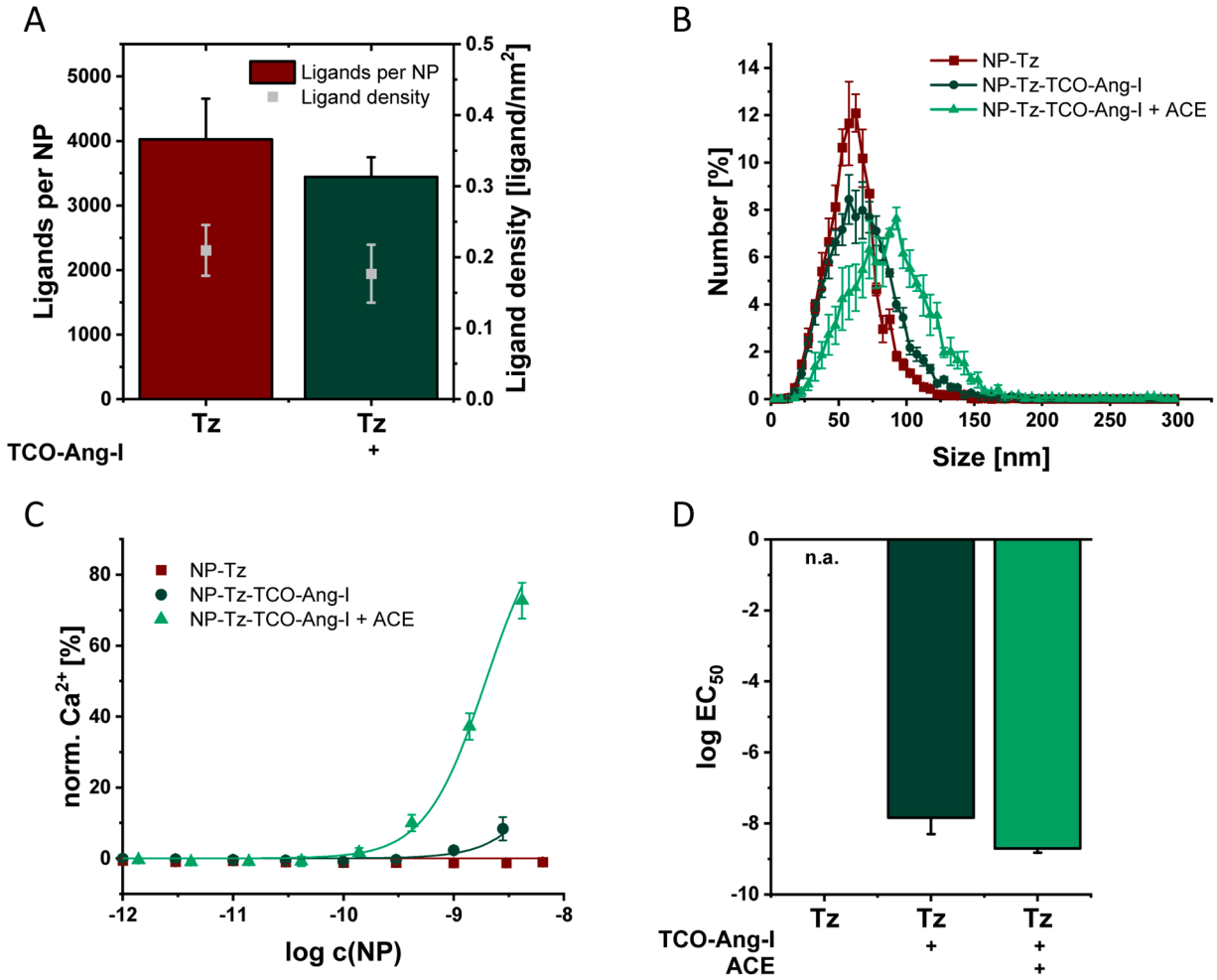

Fig. 5. Post-functionalization of NP-Tz with Ang-I via iEDDA reaction and avidity for the AT1R on rMCs. (A) Number of ligands per NP and derived ligand density before and after functionalization with Ang-I via iEDDA reaction. Tetrazine was quantified using its absorption in the visible range; Ang-I content after functionalization was determined using a BCA assay; the ligand concentrations were referred to the NP concentrations determined by NTA. (B) Size alteration of the particles by post functionalization and enzymatic processing with soluble ACE. Size distribution measured by NTA. (C) Avidity for the AT1 receptor of the tetrazine-only functionalized NPs (NP-Tz), the subsequently Ang-I functionalized NPs (NP-Tz-TCO-Ang-I) and the NPs additionally activated with soluble ACE (NP-Tz-TCO-Ang-I + ACE). Binding curves derived from Fura-2 AM Ca^{2+} mobilization assays using the direct procedure with immediate measurement of Ca^{2+} influx after addition of the cell suspension. (D) Corresponding logEC_{50} values for the NPs obtained from the fit of the Fura-2 AM Ca^{2+} assay data. Results in A are presented as mean ± SD of N = 3 independent experiments. The results in B-D are presented as mean ± SD from a single experiment with n = 3 measurements.

with Ang-I via iEDDA reaction can be activated, as required for later application, by membrane-bound ACE. The rMCs used as a model cell line exhibit a high ACE activity of approx. 0.35 pmol of hydrolyzed substrate per minute and per µg of protein (Maslanka Figueroa et al., 2019). The NPs were initially incubated with the cell suspension for 1 h, and subsequently the extent to which the influx of Ca^{2+} triggered by the addition of free Ang-II could be reduced was measured (for further explanation see **SI Figure 11**). While the NPs functionalized only with tetrazine did not bind to the AT1 receptor, the particles post-functionalized with Ang-I showed interaction at higher concentrations (see Fig. 6 A). Here, a sufficient number of Ang-I ligands appeared to have been processed to Ang-II by ACE on the cell membrane during incubation. The directly Ang-I functionalized NPs behaved similarly and also saturated the receptor at higher concentrations. NP-Ang-II, tested for comparison, where all ligands were directly available for receptor binding, showed an IC_{50} value in the picomolar range (see **SI Figure 13** for a comparison with NP-Ang-II with acetylation at the N-terminus of angiotensin). In contrast, the IC_{50} value for Ang-I functionalized NPs was in the nanomolar range. Comparable values of 2.9 ± 0.5 nM for NPs directly Ang-I functionalized and 1.5 ± 0.2 nM for NPs post-functionalized via iEDDA reaction were found. It could be concluded that the attachment of the Ang-I ligand through the iEDDA reaction did not hinder enzymatic activation and binding to the AT1R.

Intracellular calcium measurements were conducted over a 3-h period to explore the interactions between NPs and cells. The degree to which different NPs could reduce calcium signaling triggered by the addition of free agonist Ang-II served as an indicator of the extent to which these NPs had bound to the AT1 receptors. This approach allowed to observe the kinetics of these interactions. NPs lacking ligands for the AT1R, such as NP-Tz, exhibited minimal receptor binding. Conversely, particles functionalized with Ang-I through the iEDDA reaction exhibited a slow binding to the AT1 receptor. This could be attributed to the requirement for enzymatic processing of Ang-I to Ang-II on the particle before the successful interaction between NPs and the AT1 receptors on the target cell surface (Maslanka Figueroa et al., 2020). After approximately 1 h, saturation was achieved with slightly over 60 % AT1R inhibition (see Fig. 6 B). The NP-Tz incubated with cells and exposed to TCO-PEG_4-Ang-I displayed a trend similar to the particles functionalized with Ang-I via the iEDDA reaction prior to the experiment, albeit with slightly lower AT1R inhibition. In summary, it could be concluded that pre-functionalized NPs, such as NP-Tz-TCO-Ang-I, were activated to Ang-II through cell membrane-bound ACE and subsequently interact with AT1 receptors (see Fig. 6 D). This likely holds true for particles that were functionalized *in vitro* as well. Since NP-Tz did not interact with the AT1R, NPs could be activated by the addition of TCO-PEG_4-Ang-I and subsequent enzymatic processing, allowing them to bind to the AT1 receptor, potentially leading to internalization. The fundamental

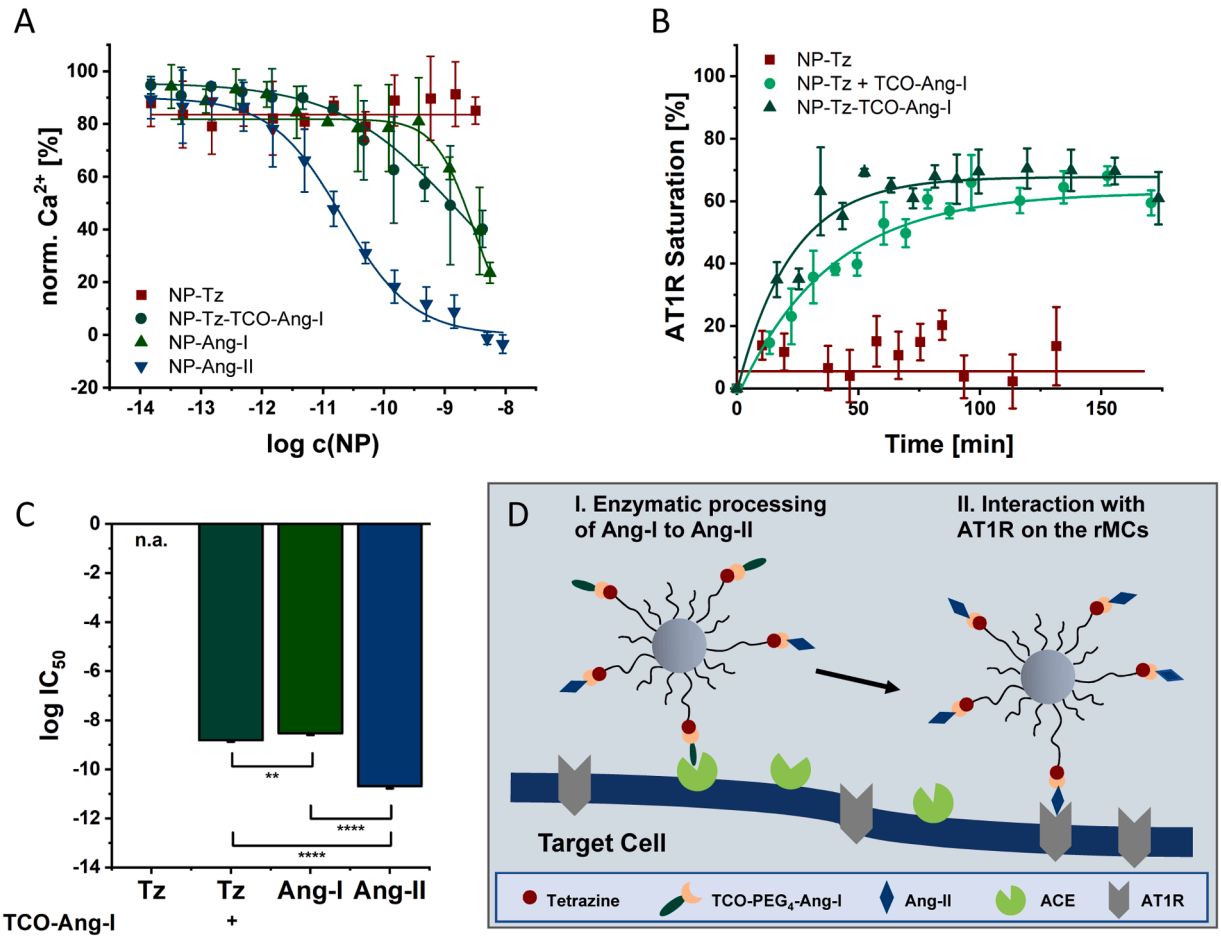

Fig. 6. Characterizing NP-cell interactions through intracellular calcium measurements. (A) Particle avidity for the AT1R after 1 h incubation with the cells. Binding curves determined via Fura-2 AM Ca^{2+} mobilization assay by inverse stimulation with free Ang-II. (B) Investigation of the kinetics of NP-cell interaction by determination of AT1R binding over time. The particles investigated included those functionalized only with tetrazine (NP-Tz), tetrazine-functionalized NPs that were already incubated with the cells and exposed to TCO-Ang-I *in vitro* (NP-Tz + TCO-Ang-I), and particles functionalized with Ang-I post-experimentally (NP-Tz-TCO-Ang-I). (C) logIC_{50} values for the NPs obtained from the fit of the Fura-2 AM Ca^{2+} assay data. (D) Scheme of NP-cell interaction with enzymatic processing and subsequent binding to the AT1R. Results in A and C are presented as mean ± SD of N = 3 independent experiments. Results in B are presented as mean ± SD of n = 3 measurements from one experiment.

requirement for a switchable particle was established.

4. Conclusion

We demonstrated that NPs can be rendered switchable with respect to their interaction with a receptor through an external chemical stimulus. The combination of iEDDA reaction for subsequent NP functionalization and ectoenzyme-based ligand activation allows for specific particle tailoring. Scenarios wherein the stealth effect of non-functionalized NPs is initially leveraged for prolonged circulation, followed by temporally controlled identification of target cells, are conceivable. This approach may potentially reduce off-target accumulations and enhance the efficacy of NPs for drug delivery. The iEDDA reaction, as a rapid and robust bioorthogonal reaction, proved to be well-suited for ligand conjugation, facilitating the creation of ligand-switchable particles. The additional processing of ligands by an ectoenzyme offers the advantage of minimizing biological effects prior to activation. Furthermore, two-step recognition involving ectoenzyme and the receptor to which subsequent binding is desired enhances specificity for the target cell. In general, this proof-of-concept study can be regarded as an initial step in exploring the potential of the iEDDA reaction for the switchable design of NPs.

Associated content

Supporting Information: Details regarding the synthesis of PLA-PEG block copolymers and the tetrazine ligand, coupling of the ligands, synthesis of TCO-PEG$_4$-Ang-I and TCO-AcAng-I, preparation and characterization of the polymer NPs, PEG conformation on the NP surface, considerations on iEDDA reaction kinetics, remarks on the direct and inverse procedure of the Ca^{2+} mobilization assay, comparison of non-acetylated and acetylated angiotensin (pdf).

CRediT authorship contribution statement

Johannes Lang: Writing – original draft, Visualization, Validation, Methodology, Investigation, Formal analysis, Conceptualization. **Kathrin Schorr:** Writing – review & editing. **Achim Goepferich:** Writing – review & editing, Supervision, Project administration, Funding acquisition, Conceptualization.

Declaration of competing interest

The authors declare that they have no known competing financial interests or personal relationships that could have appeared to influence the work reported in this paper.

Acknowledgment

The authors want to thank Prof. Miriam Breunig, Felix Baumann, Melanie Walter, Stephan Melchner, and Oliver Zimmer for their continuous constructive discussions on the conducted research. Further, the authors would like to acknowledge the excellent technical assistance of Renate Liebl in cell culture and Chrismarie Grace Faltermeier in the synthesis of block copolymers and ligand couplings. The authors thank Mona Lex for her support in NP preparation and characterization during her research internship. Moreover, the authors are grateful for the opportunity to use the preparative HPLC at the Department of Pharmaceutical and Medicinal Chemistry II at the University of Regensburg and for the technical support from Beate Hoffelner.

Supplementary materials

Supplementary material associated with this article can be found, in the online version, at doi:10.1016/j.ejps.2024.106944.

Data availability

Data will be made available on request.

References

Mitchell, MJ, Billingsley, MM, Haley, RM, Wechsler, ME, Peppas, NA, Langer, R, 2021. Engineering precision nanoparticles for drug delivery. Nat. Rev. Drug Discov. 20 (2), 101–124. https://doi.org/10.1038/s41573-020-0090-8.

Zhao, Z, Ukidve, A, Krishnan, V, Mitragotri, S, 2019. Effect of physicochemical and surface properties on *in vivo* fate of drug nanocarriers. Adv. Drug Deliv. Rev. 143, 3–21. https://doi.org/10.1016/j.addr.2019.01.002.

Li, X, Montague, EC, Pollinzi, A, Lofts, A, Hoare, T, 2022. Design of smart Size-, Surface-, and shape-switching nanoparticles to improve therapeutic efficacy. Small. 18 (6), e2104632. https://doi.org/10.1002/smll.202104632.

Blanco, E, Shen, H, Ferrari, M, 2015. Principles of nanoparticle design for overcoming biological barriers to drug delivery. Nat. Biotechnol. 33 (9), 941–951. https://doi.org/10.1038/nbt.3330.

Lu, Q, Yu, H, Zhao, T, Zhu, G, Li, X, 2023. Nanoparticles with transformable physicochemical properties for overcoming biological barriers. Nanoscale 15 (32), 13202–13223. https://doi.org/10.1039/D3NR01332D.

Jin, Q, Deng, Y, Chen, X, Ji, J, 2019. Rational design of cancer nanomedicine for simultaneous stealth surface and enhanced cellular uptake. ACS. Nano 13 (2), 954–977. https://doi.org/10.1021/acsnano.8b07746.

Mura, S, Nicolas, J, Couvreur, P, 2013. Stimuli-responsive nanocarriers for drug delivery. Nature Mater. 12 (11), 991–1003. https://doi.org/10.1038/nmat3776.

Crucho, CIC, 2015. Stimuli-responsive polymeric nanoparticles for nanomedicine. ChemMedChem. 10 (1), 24–38. https://doi.org/10.1002/cmdc.201402290.

Su, Y, Jin, G, Zhou, H, Yang, Z, Wang, L, Mei, Z, Jin, Q, Lv, S, Chen, X, 2023. Development of stimuli responsive polymeric nanomedicines modulating tumor microenvironment for improved cancer therapy. Med. Rev. 3 (1), 4–30. https://doi.org/10.1515/mr-2022-0048.

Yao, Q, Kou, L, Tu, Y, Zhu, L, 2018. MMP-responsive 'Smart' drug delivery and tumor targeting. Trends. Pharmacol. Sci. 39 (8), 766–781. https://doi.org/10.1016/j.tips.2018.06.003.

He, Y, Lei, L, Cao, J, Yang, X, Cai, S, Tong, F, Huang, D, Mei, H, Luo, K, Gao, H, He, B, Peppas, NA, 2021. A combinational chemo-immune therapy using an enzyme-sensitive nanoplatform for dual-drug delivery to specific sites by cascade targeting. Sci. Adv. 7 (6). https://doi.org/10.1126/sciadv.aba0776.

Cao, Z, Li, D, Wang, J, Yang, X, 2021. Reactive oxygen species-sensitive polymeric nanocarriers for synergistic cancer therapy. Acta Biomater. 130, 17–31. https://doi.org/10.1016/j.actbio.2021.05.023.

Wang, S, Yu, G, Wang, Z, Jacobson, O, Lin, L-S, Yang, W, Deng, H, He, Z, Liu, Y, Chen, Z-Y, Chen, X, 2019. Enhanced antitumor efficacy by a cascade of reactive oxygen species generation and drug release. Angewandte Chemie Int. Edit. 58 (41), 14758–14763. https://doi.org/10.1002/anie.201908997.

Deng, J, Walther, A, 2020. ATP-responsive and ATP-Fueled self-assembling systems and materials. Adv. Mater. 32 (42), e2002629. https://doi.org/10.1002/adma.202002629.

Yu, M, Zeng, W, Ouyang, Y, Liang, S, Yi, Y, Hao, H, Yu, J, Liu, Y, Nie, Y, Wang, T, Deng, Y, Wu, M, 2022. ATP-exhausted nanocomplexes for intratumoral metabolic intervention and photoimmunotherapy. Biomaterials 284, 121503. https://doi.org/10.1016/j.biomaterials.2022.121503.

Tao, Y, Chan, HF, Shi, B, Li, M, Leong, KW, 2020. Light: a magical tool for controlled drug delivery. Adv. Funct. Mater. 30 (49), 2005029. https://doi.org/10.1002/adfm.202005029.

Sponchioni, M, Capasso Palmiero, U, Moscatelli, D, 2019. Thermo-responsive polymers: applications of smart materials in drug delivery and tissue engineering. Mater. Sci. Eng. C. Mater. Biol. Appl. 102, 589–605. https://doi.org/10.1016/j.msec.2019.04.069.

Tu, L, Liao, Z, Luo, Z, Wu, Y-L, Herrmann, A, Huo, S, 2021. Ultrasound-controlled drug release and drug activation for cancer therapy. Exploration 1 (3), 20210023. https://doi.org/10.1002/EXP.20210023.

Li, H, Miteva, M, Kirkbride, KC, Cheng, MJ, Nelson, CE, Simpson, EM, Gupta, MK, Duvall, CL, Giorgio, TD, 2015. Dual MMP7-proximity-activated and folate receptor-targeted nanoparticles for siRNA delivery. Biomacromolecules. 16 (1), 192–201. https://doi.org/10.1021/bm501394m.

Jin, E, Zhang, B, Sun, X, Zhou, Z, Ma, X, Sun, Q, Tang, J, Shen, Y, van Kirk, E, Murdoch, WJ, Radosz, M, 2013. Acid-active cell-penetrating peptides for *in vivo* tumor-targeted drug delivery. J. Am. Chem. Soc. 135 (2), 933–940. https://doi.org/10.1021/ja311180x.

Oliveira, BL, Guo, Z, Bernardes, GJL, 2017. Inverse electron demand Diels-Alder reactions in chemical biology. Chem. Soc. Rev. 46 (16), 4895–4950. https://doi.org/10.1039/C7CS00184C.

Idiago-López, J, Moreno-Antolín, E, de, La Fuente JM, Fratila, RM, 2021. Nanoparticles and bioorthogonal chemistry joining forces for improved biomedical applications. Nanoscale Adv. 3 (5), 1261–1292. https://doi.org/10.1039/D0NA00873G.

Hennig, R, Pollinger, K, Tessmar, J, Goepferich, A, 2015. Multivalent targeting of AT1 receptors with angiotensin II-functionalized nanoparticles. J. Drug Target. 23 (7-8), 681–689. https://doi.org/10.3109/1061186X.2015.1035276.

Maslanka Figueroa, S, Veser, A, Abstiens, K, Fleischmann, D, Beck, S, Goepferich, A, 2019. Influenza A virus mimetic nanoparticles trigger selective cell uptake. Proc. Natl. Acad. Sci. U S. A 116 (20), 9831–9836. https://doi.org/10.1073/pnas.1902563116.

Abstiens, K, Goepferich, AM, 2019. Microfluidic manufacturing improves polydispersity of multicomponent polymeric nanoparticles. J. Drug Deliv. Technol. 49, 433–439. https://doi.org/10.1016/j.jddst.2018.12.009.

Abstiens, K, Maslanka Figueroa, S, Gregoritza, M, Goepferich, AM, 2019. Interaction of functionalized nanoparticles with serum proteins and its impact on colloidal stability and cargo leaching. Soft. Matter. 15 (4), 709–720. https://doi.org/10.1039/C8SM02189A.

Clayton, KN, Salameh, JW, Wereley, ST, Kinzer-Ursem, TL, 2016. Physical characterization of nanoparticle size and surface modification using particle scattering diffusometry. Biomicrofluidics. 10 (5). https://doi.org/10.1063/1.4962992.

Zimmer, O, Goepferich, A, 2023. How clathrin-coated pits control nanoparticle avidity for cells. Nanoscale Horiz. 8 (2), 256–269. https://doi.org/10.1039/D2NH00543C.

Filipe, V, Hawe, A, Jiskoot, W, 2010. Critical evaluation of Nanoparticle Tracking Analysis (NTA) by NanoSight for the measurement of nanoparticles and protein aggregates. Pharm. Res. 27 (5), 796–810. https://doi.org/10.1007/s11095-010-0073-2.

Grynkiewicz, G, Poenie, M, Tsien, RY, 1985. A new generation of Ca2+ indicators with greatly improved fluorescence properties. J. Biol. Chem. 260 (6), 3440–3450.

Maslanka Figueroa, S, Fleischmann, D, Beck, S, Goepferich, A, 2020. The effect of ligand mobility on the cellular interaction of multivalent nanoparticles. Macromol. Biosci. 20 (4), e1900427. https://doi.org/10.1002/mabi.201900427.

Yang, Q, Jones, SW, Parker, CL, Zamboni, WC, Bear, JE, Lai, SK, 2014. Evading immune cell uptake and clearance requires PEG grafting at densities substantially exceeding the minimum for brush conformation. Mol. Pharm. 11 (4), 1250–1258. https://doi.org/10.1021/mp400703d.

Darko, A, Wallace, S, Dmitrenko, O, Machovina, MM, Mehl, RA, Chin, JW, Fox, JM, 2014. Conformationally strained trans-Cyclooctene with improved stability and excellent reactivity in Tetrazine ligation. Chem. Sci. 5 (10), 3770–3776. https://doi.org/10.1039/C4SC01348D.

Karver, MR, Weissleder, R, Hilderbrand, SA, 2011. Synthesis and evaluation of a series of 1,2,4,5-tetrazines for bioorthogonal conjugation. Bioconjug. Chem. 22 (11), 2263–2270. https://doi.org/10.1021/bc200295y.

Leenson, IA, 1999. Old rule of thumb and the arrhenius equation. J. Chem. Educ. 76 (10), 1459. https://doi.org/10.1021/ed076p1459.

Kramer, S, Svatunek, D, Alberg, I, Gräfen, B, Schmitt, S, Braun, L, van Onzen, AHAM, Rossin, R, Koynov, K, Mikula, H, Zentel, R, 2019. HPMA-based nanoparticles for fast, Bioorthogonal iEDDA ligation. Biomacromolecules 20 (10), 3786–3797. https://doi.org/10.1021/acs.biomac.9b00868.

Maslanka Figueroa, S, Fleischmann, D, Beck, S, Tauber, P, Witzgall, R, Schweda, F, Goepferich, A, 2020. Nanoparticles mimicking viral cell recognition strategies are superior transporters into Mesangial cells. Adv. Sci. 7 (11), 1903204. https://doi.org/10.1002/advs.201903204.